JAASCI
http://jaasci.com
JOURNAL OF ADVANCED APPLIED SCIENCES
e-ISSN: 2979-9759
PRENSİP
https://prensip.gen.tr

RESEARCH ARTICLE

Gas Sensing Performance of Hydrothermally Produced ZnO Nanostructures Based on Dip-Coated Seed Layers with Different Dipping Cycles

Ahmad Ajjaq[1*] • Ali Orkun Çağırtekin[1] • Özlem Barin[1,2] • Irmak Karaduman Er[3] • Selim Acar[1]

[1]Gazi University, Faculty of Science, Department of Physics, Ankara/Türkiye
[2]Yüksek İhtisas University, Vocational School of Health Services, Opticianry Program, Ankara/Türkiye
[3]Çankırı Karatekin University, Eldivan Medical Services Vocational School, Department of Medical Services and Techniques, Çankırı/Türkiye

ARTICLE INFO

Article History
Received: 11.10.2022
Accepted: 28.10.2022
First Published: 07.12.2022

Keywords
Dip coating
Gas sensor
Hydrothermal
Zinc oxide

ABSTRACT

It is admitted that synthesis methods and their relative parameters have a crucial effect on the size of the produced nanoparticles, surface area/volume ratio, porosity as well as defects in the film which in turn affect the morphology and thus the ultimate performance of the fabricated gas sensor. In this study, ZnO films were synthesized for gas sensing applications using a hydrothermal technique based on dip-coated seed layers with different number of dipping cycles. The effect of the number of dipping cycles in seed layers on the structural, morphological and gas sensing properties of the hydrothermally synthesized ZnO films was investigated respectively using X-ray diffraction patterns, scanning electron microscope images and gas sensing measurements. The increase in the number of dipping cycles deteriorated the crystal quality of the subsequent hydrothermal growth and adversely affected the gas sensing performance of the produced films. Actually, the increment in the number of dipping cycles caused a decrease in the sensitivity of the sensors at all investigated operating temperatures and for all investigated gas concentrations. The structural and morphological variations that happened due to the number of dipping cycles in the seed layers were correlated with the gas sensing properties of the produced films for a better comprehensive understanding.

Please cite this paper as follows:

Ajjaq, A., Çağırtekin, A. O., Barin, Ö., Karaduman Er, I., & Acar, S. (2022). Gas sensing performance of hydrothermally produced ZnO nanostructures based on dip-coated seed layers with different dipping cycles. *Journal of Advanced Applied Sciences*, *1*(1), 8-15. https://doi.org/10.29329/jaasci.2022.476.02

Introduction

The huge rise in greenhouse gases' levels in the atmosphere and its destructive effects on all living species have alarmed researchers to look for possible ways to reduce the emission of greenhouse gases resulting mainly from the combustion of fossil fuels. One of the ways researchers have come up with is the use of hydrogen gas as an energy source instead of fossil fuels. In this context, the importance of hydrogen gas is increasing daily, and its exploitation became an interesting subject upon which researchers are conducting experiments. Although hydrogen gas has advantageous features such as being light compared to air, having zero carbon emission, being non-toxic and environmentally friendly, it can be dangerous depending on the area of use because it has no color, taste and smell. The fact that it is explosive in cases of gas leakages and

* Corresponding author
E-mail address: ahmad.ajjaq@gazi.edu.tr

can be poisoning at high concentrations sheds light on the importance of gas sensors that can detect hydrogen gas in air before any possible occurrence of a disaster.

With the developing technology, the use of nanostructured materials (especially those based on metal oxide semiconductors) as circuit elements in electronic devices like gas sensors increased rapidly. This has pushed researchers to investigate nanostructured materials in many aspects according to their purpose of use. As for gas sensors, it is important for human and environmental safety to develop metal oxide nanostructured sensing materials with high sensitivity, low limit of detection, and fast response. Zinc oxide (ZnO) materials are evidenced to be one of the most promising metal oxide materials due to their improved gas detection performance owing to several advantageous features such as its direct wide band gap, high lifetime, and good stability. ZnO materials can be produced by various synthesis methods such as successive ionic layer adsorption and deposition method (Soltabayev et al., 2022), dip coating method (Al Farsi et al., 2021), spin-coating method (Raghu et al., 2018), chemical bath deposition method (Poornajar et al., 2016), hydrothermal method (Sansenya et al., 2022), magnetron sputtering method (Gao & Li, 2004), and spray pyrolysis method (Saha et al., 2020). Amudhavalli et al. (2022) have presented a recent review on the optimized deposition parameters with each method for the synthesis of high-quality ZnO thin films. Production methods and production parameters within each method can influence (improve or worsen) to a big extent the gas sensing properties of ZnO nanostructured materials.

In this study, gas sensors were fabricated by a combination of dip coating and hydrothermal treatment techniques. The effect of the number of dipping cycles on the structural, morphological and gas detection performance of the synthesized samples was investigated with an aim to optimize the dip coating cycle number in future hydrothermal fabrications for gas sensing applications. The structural and morphological changes triggered by the number of dipping cycles were correlated with the obtained gas sensing properties for a comprehensive understanding of the results.

Materials and Methods

Sensor Fabrication

The sensing films were coated on microscope glass slides (5 mm × 12 mm) in two phases. Before any coating was done, the glass substrates were thoroughly cleaned with soapy water and then washed in an ultrasonic bath for 10 minutes using ethanol, acetone, and distilled water, respectively. In the first phase of the coating process, ZnO thin film layers were grown on the glass substrates to serve as nucleation layers for subsequent growth. The layers were grown in 5 and 10 cycles by the dip coating method where each cycle consists of three consecutive steps: immersion in the solution [0.3 M of zinc acetate $Zn(OAc)_2$, 33 mL of methanol, 0.5 mL of monoethanolamine MEA] for 2 s, heating in the oven (≈300 ºC) for 3 min, and holding in the air (RT) for 2 min. The coated layers were annealed at 500 ºC for 30 min in an air environment and left to rest for one day before further treatment. In the second phase of the coating process, the seed-coated substrates were placed in 50 mL Teflon containers with a well-mixed 0.01 M of $Zn(OAc)_2$, distilled water, and 1:1 of hexamethylenetetramine HMTA. The Teflon containers were put in hydrothermal reactors and subjected to hydrothermal treatment at 70 ºC for 1 h. The samples were finally rinsed with distilled water and left to rest for one day before being annealed again at 500 ºC for 30 min in an air environment. The sensors were then fabricated by a thermal evaporation method using an interlinked electrode mask (width: 45 µm, length: 2.5 mm, and spacing: 90 µm) with high purity (99.99%) silver as source material. The samples/sensors will be denoted as D5 (denoting 5 dipping cycles) and D10 (denoting 10 dipping cycles) throughout the manuscript. The phases of the experimental synthesis procedure are summarized in Figure 1.

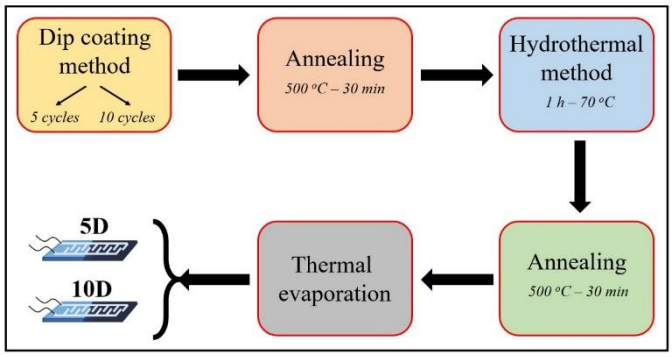

Figure 1. A map diagram of the experimental synthesis procedure.

Measurement Methods

The structural properties of the produced samples were explored using X-ray diffraction (XRD) measurements taken by the D8 Advance device with a CuKα1 source from 20º to 90º in 0.02º incremental steps of the diffraction angle. The morphological characterization of the samples was done based on the surface and cross-sectional field emission scanning electron microscope (FE-SEM) images taken by the Hitachi SU5000 device using the secondary detector at an applied voltage of 10 kV. The cross-sectional FE-SEM images were collected following an appropriate gold coating in argon medium using the Leica EM ACE200 device. Gas sensing performance of the fabricated sensors was analyzed using a homemade computer-controlled gas measurement system comprising a stainless steel test cell, two MKS branded mass flow controllers [one for the target gas (5 SCCM) and one for dry air (500 SCCM)], Keithley 2400 current-voltage analyzer and SRS-CTC100 temperature controller. The measurement settings were set as follows: gas on = 10 min, gas off = 20 min,

CC BY

permanent steady circulation of dry = yes, voltage = 1 V, and relative humidity = 40%.

Results and Discussion

Structural Analysis

Figure 2 displays the measured X-ray diffraction patterns of the produced samples. All the detected peaks are well-indexed with the hexagonal wurtzite crystalline structure of ZnO (Card No. 00-036-1451). Ten well-defined diffraction peaks were detected in the D5 sample with high intensity at 2θ = 31.71º, 34.45º, 36.14º, 47.39º, 56.54º, 62.81º, 66.35º, 67.83º, 68.93º and 72.48º, and were indexed respectively to the (100), (002), (101), (102), (110), (103), (200), (112), (201) and (004) diffraction planes with a preferential orientation along the (002) direction. In the D10 sample, however, only five diffraction peaks with very low intensity were detected at 2θ = 31.45º, 34.10º, 35.92º, 56.17º and 62.58º, and were indexed respectively to the (100), (002), (101), (110) and (103) diffraction planes. Clearly, the intensity of the diffraction peaks decreased greatly and the peaks shifted slightly to lower diffraction angles with the increase in the number of dipping cycles applied to the dip-coated nucleation layers. Here, the left shift of diffraction peaks can be attributed to changes in the lattice microstructure parameters like crystallite size and strain, and it precisely implies an expansion in the lattice parameters as is confirmed by the Scherrer formulation below. A clear deterioration in crystal quality can be seen in the D10 sample from which it can be deduced that five dipping cycles in the nucleation layer are more appropriate for subsequent hydrothermal reactions. The crystallite size and microstrain values of the produced samples were estimated by Scherrer formulation using Equations (1) and (2) respectively (Cura et al., 2021),

$$D = \frac{K\lambda}{\beta \cos\theta} \quad (1)$$

$$\varepsilon = \frac{\beta}{4 \tan\theta} \quad (2)$$

where K, λ, β and θ are well-known parameters. In Eq. (1), K was set to 0.94 and λ was taken as 1.5406 Å. The average crystallite size increased from 241 Å in the D5 sample to 272 Å in the D10 sample while the microstrain decreased slightly from 4.95×10^{-3} in the D5 sample to 4.75×10^{-3} in the D10 sample. Based on the crystallite size-strain analysis done, it can be deduced that more dipping cycles or equivalently higher reaction times trigger an increase in crystallite size and decrease in lattice strain of the hydrothermally synthesized film. Similar increasing trend in crystallite size of ZnO films with the increase in dipping cycles was reported earlier in the literature by Toe et al. (2021) using dip coating, Atay and Gultepe (2021) using spin coating, and Devi et al. (2019) using SILAR coating.

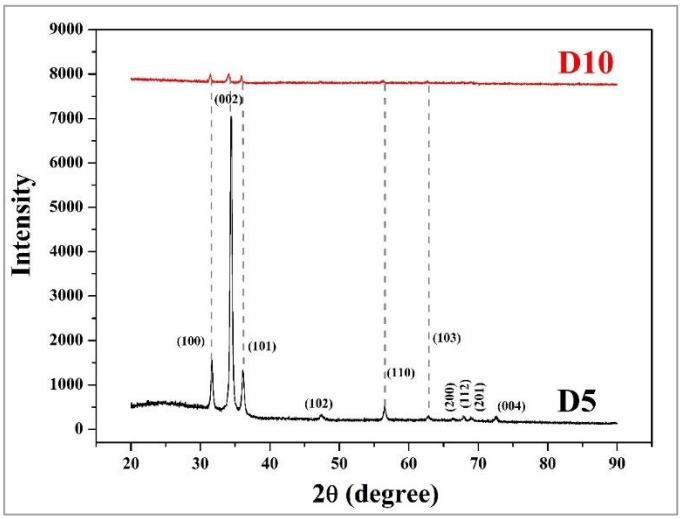

Figure 2. XRD patterns of the synthesized films.

Morphological Analysis

The top- and side-view FESEM images of the hydrothermally synthesized samples and their corresponding seed layers are given in Figure 3. It is clearly seen that seed layers are homogenously coated on glass substrates in both samples. Five dipping cycles caused the formation of a seed layer with a thickness of about 123 nm while ten dipping cycles caused the formation of a seed layer with a thickness of about 201 nm. It is noteworthy that the appropriate use of dip coating technique can yield promising results in terms of the formation of homogeneous thin film coatings for several applications. After the hydrothermal treatment of the synthesized seed coatings, the cross-section thickness of the overall coated film increased to about 160 nm in the D5 sample and 253 nm in the D10 sample. With the hydrothermal reaction, nanorods started to form from the nucleation sites in the seed layers. However, the samples were not exposed to enough temperature and time which proves the absence of well-formed rod-like structures. These results are consistent with the studies done by Kaya et al. (2020), Kamruzzaman and Zapien (2018), and Amin et al. (2011) who reported that the proper hydrothermal nucleation of nanorods happens at a threshold temperature of 75 ºC and threshold time of 1 h. The diameter of the rods to be grown increased from about 27 nm in the D5 sample to about 37 nm in the D10 sample and caused an increase in agglomeration and decrease in voids among the rods to be grown. Considering the high surface area to volume ratio in the D5 sample compared to the D10 sample, it could be speculated that the former may have a better gas sensing performance.

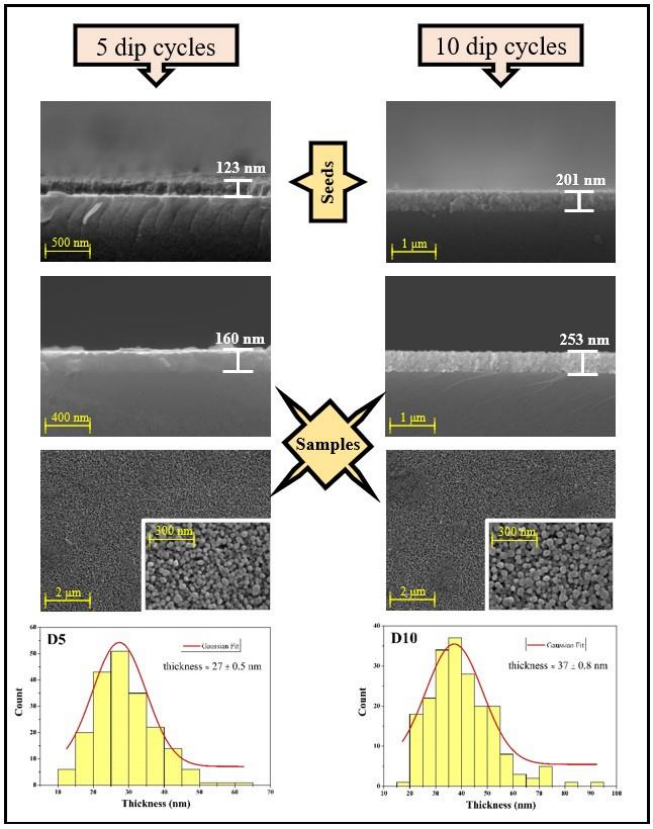

Figure 3. Top- and side-view FESEM images of the synthesized films.

Gas Sensing Analysis

The working temperature at which a gas sensor shows maximum sensitivity defines the optimal working temperature of the sensor. The increase in temperature causes the kinetic energy of the target gas molecules sent to the sensor surface to increase. Increasing the temperature also causes the surface reactions to accelerate, thus increasing the sensitivity of the sensor up to some limit. This is because sensors operating at high temperatures consume high power consumption, thus causing the sensor's sensing surface to deteriorate. As a first step in examining the gas detection performance of the produced sensors, gas detection measurements were made for 50 ppm concentration of H_2 gas in the temperature range of 30 ºC to 270 ºC in 20 ºC steps in order to determine the optimum operating temperature of each sensor. The estimated sensitivity of each sensor versus the working temperature is given in Figure 4. The sensitivity was estimated according to the formula (Ghosh et al., 2020),

$$S = \frac{|R_g - R_a|}{R_a} \times 100 \quad (3)$$

where R_a and R_g represent respectively the baseline resistance of the sensor in dry air and the saturation resistance of the sensor in exposure to the target gas. The threshold working temperature at which the sensors started responding to 50 ppm H_2 gas was 170 ºC for the D5 sensor (with about 5% sensitivity) and 190 ºC for the D10 sensor (with about 2% sensitivity). With the gradual increase in temperature, the response of both sensors increased up to a maximum of about 27% (for the D5 sensor) and about 10% (for the D10 sensor) at 230 ºC. The temperature of 230 ºC was noted as the optimal working temperature of both fabricated sensors. Beyond the optimal working temperature, a decrease in sensitivity was observed in both sensors with a further increase in temperature. This behavior can be attributed to the dissociation and adsorption processes of oxygen ions on the sensing surface depending on the temperature which was elaborated in detail in the previous study (Barin et al., 2022). The gas sensing measurements were terminated at 270 ºC because a clear dropdown in sensitivity was revealed in both sensors. It is noteworthy that the same D5 sensor produced in a 3 h - 90 ºC hydrothermal reaction showed an elevated response to H_2 gas of about 36% at the same optimal working temperature (Barin et al., 2022). This emphasizes the threshold and optimal synthesis parameters of the hydrothermal route for gas sensing applications. The higher response of the D5 sensor can be attributed to its preferable structural ad morphological properties compared to the D10 sample. Based on the XRD results, the D5 sample exhibited a better crystalline structure with a smaller crystallite size. It is generally reported that the smaller the crystallite size is, the better the gas sensing performance becomes (Xu et al., 2000; Altun et al., 2021; Barin et al., 2022). And according to the SEM images, the D5 sample showed a greater surface area-to-volume ratio which is usually favorable for achieving a good gas sensing performance. It is noteworthy to mention that in this study, gas-sensing properties of the ZnO nanorods to be formed by the hydrothermal method on dip-coated ZnO seed layers were primarily investigated. It was demonstrated that the change in the number of dipping cycles in the dip-coated ZnO seed layer has a remarkable effect on the structure and morphology of the nanostructures produced by the hydrothermal method which ultimately influenced gas sensing properties of the hydrothermally produced film. Yet, due to the sparse nature of the hydrothermally produced nanostructures, it is thought that gas molecules can diffuse all the way down to the seed layers which also makes seed layers enroll in the gas adsorption-desorption processes of the produced samples.

CC BY

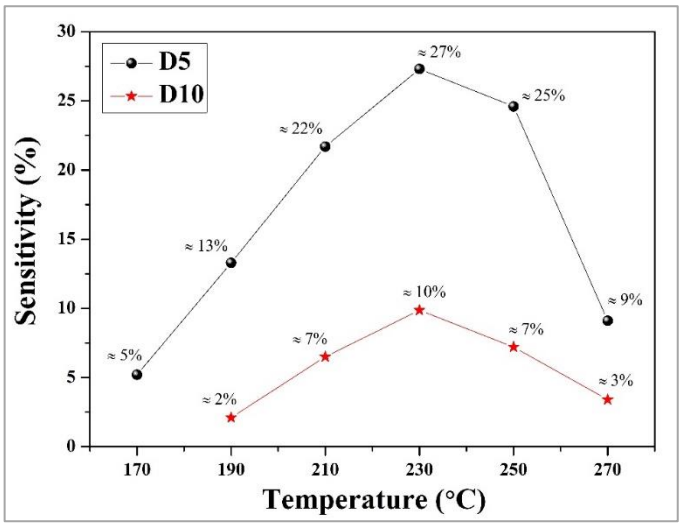

Figure 4. Sensitivity of the fabricated sensors versus working temperature.

The transient plots of the change of resistance of the fabricated sensors with time upon exposure to 50 ppm of H_2 gas at the determined optimal working temperature of 230 ºC are given in Figure 5. Using these plots, the corresponding transient sensitivities of the produced sensors were estimated and overlaid for better comparison from which response and recovery times of both sensors were calculated based on 90% arrival for the maximum sensitivity value (for response time) and 90% return to the initial baseline value (for recovery time). With exposure to H_2 gas, an instant decrease in resistance was revealed by both sensors followed by a re-increase to the initial resistance level with the cut of the target gas emission. Clearly again, while the fabricated D5 sensor showed a 27% sensitivity, the D10 sensor showed a 10% sensitivity at the optimal operating temperature. Moreover, response and recovery times are essential parameters in gas detection applications. At the optimal working temperature, both sensors showed approximately a 3 min response time with about 5 min recovery time for the D5 sensor and 2 min recovery time for the D10 sensor. The detection and recovery mechanisms of the fabricated sensors can be considered to be quite fast for hydrogen gas sensation. The results obtained in this study were compared with other reported results in Table 1.

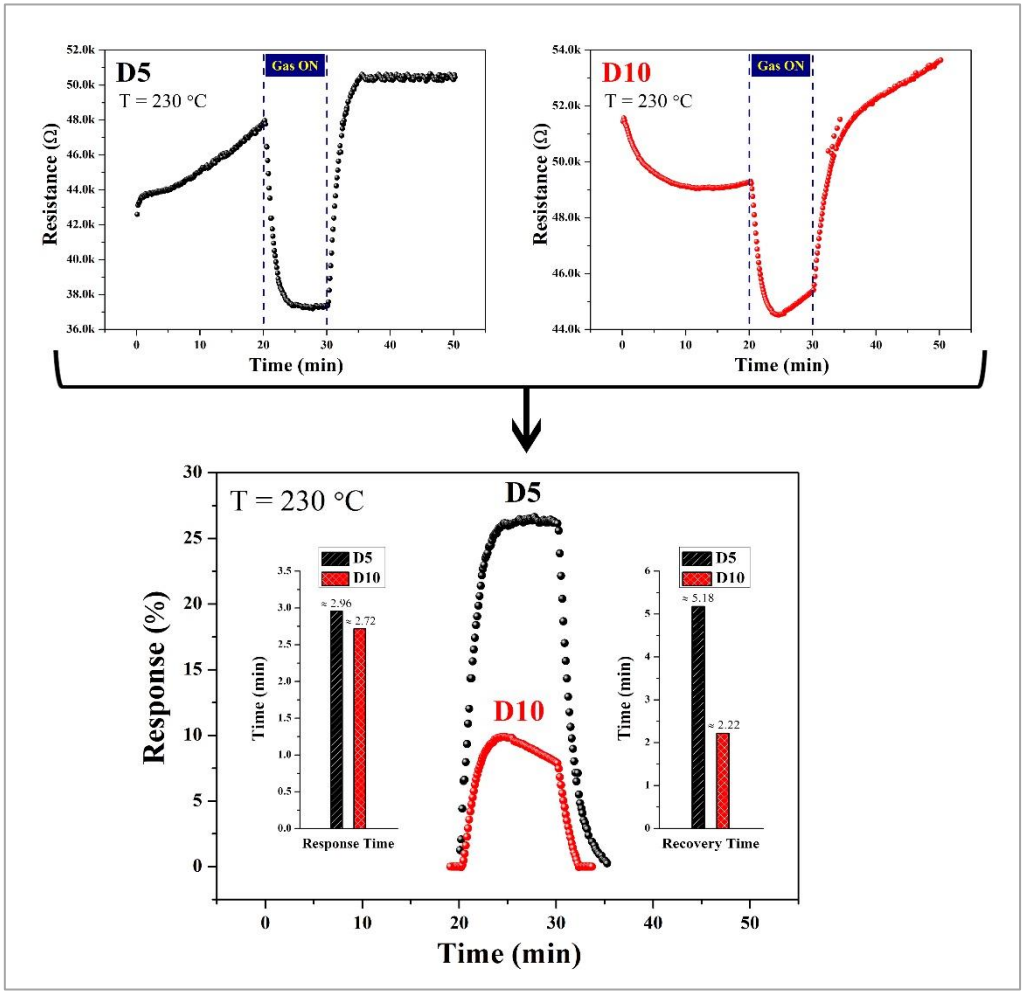

Figure 5. Transient resistance plots of the fabricated sensors at 230 ºC.

CC BY

Table 1. Literature review of some hydrothermally-grown pure ZnO films for H_2 gas sensing.

Material	Seed layer		Hydrothermal parameters		Sensor working temperature	H_2 level Sensitivity	Response/recovery times	Ref.
	Fabrication method	Cycle number	Time	Temperature				
ZnO	SILAR	40	3 h	90 ºC	190 ºC	50 ppm 25%	6 min /16 min	(Barin et al., 2022)
	Spin	5	3 h	90 ºC	270 ºC	50 ppm 51%	2 min /5 min	
	Dip	5	3 h	90 ºC	230 ºC	50 ppm 36%	3 min /7 min	
ZnO	Magnetron sputtering	Thickness = 150 nm	3 h	90 ºC	180 ºC	500 ppm 264%	2 min /2 min	(Mohammad et al., 2016)
ZnO	Dip	5	1 h	70 ºC	230 ºC	50 ppm 27%	3 min /5 min	This work
		10	1 h	70 ºC	230 ºC	50 ppm 10%	3 min /2 min	

The dynamic gas measurements of the fabricated sensors at the optimal working temperature are performed and the results are given in Figure 6 in terms of the estimated sensitivity. The sensors were exposed to 1 ppm, 5 ppm, 10 ppm, 50 ppm and 100 ppm of H_2 gas successively for 10 min and were allowed to recover for 20 min after each exposure. Clearly, the sensitivity of the sensors increased with the increase in gas concentration. The sensors showed acceptable sensitivity towards 1 ppm of H_2 gas at the optimal working temperature: about 9% (D5 sensor) and 5% (D10 sensor). The sensitivities recorded towards the 50 ppm concentration were found to be about 28% (for the D5 sensor) and 10% (for the D10 sensor). These results are in a very good agreement with the previous temperature-dependent measurements (Figure 4) reflecting the good stability of the fabricated sensors.

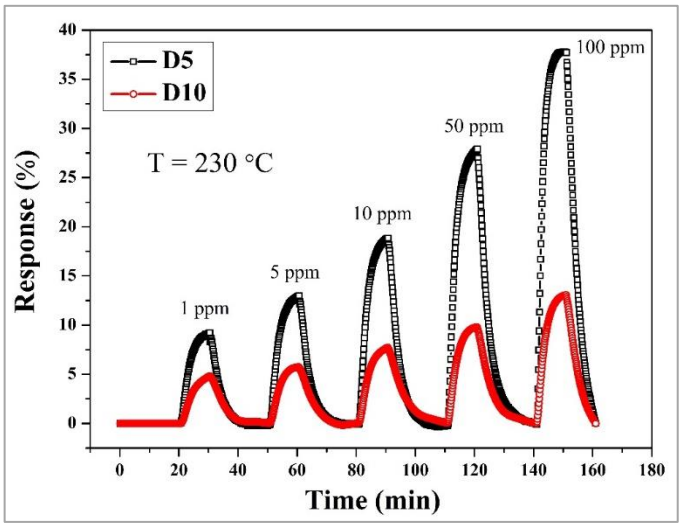

Figure 6. Dynamic plots of the fabricated sensors at 230 ºC.

The selectivity of both produced sensors to H_2 gas was examined using a set of target gases, like carbon monoxide, carbon dioxide, ammonia, acetone and methanol. For this aim, the sensors were exposed to 50 ppm of each gas at the optimal working temperature, and the sensitivity of the sensors towards each gas was estimated and provided in the radar plot given in Figure 7. Both sensors exhibited a good selectivity towards H_2 gas at 230 ºC. The estimated approximate sensitivities of the produced D5 and D10 sensors are respectively as follows: 11% and 4% (towards carbon monoxide), 5% and 3% (towards carbon dioxide), 4% and 2% (towards ammonia), 2% and 0% (towards acetone), and 1% and 0% (towards methanol).

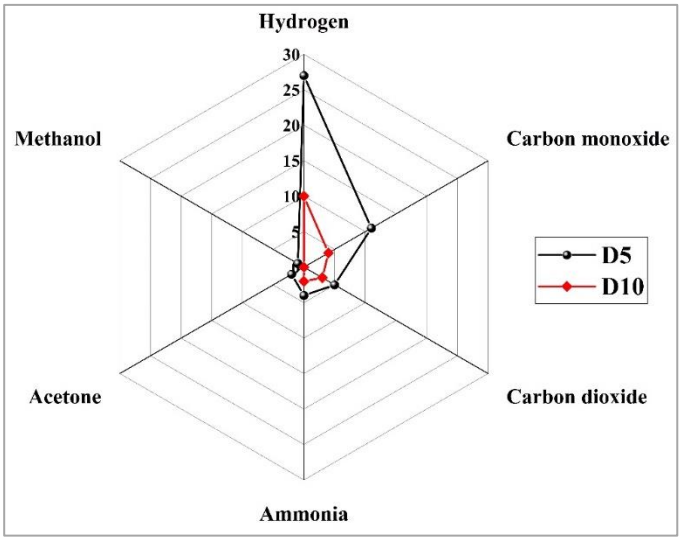

Figure 7. Selectivity plot of the fabricated sensors at 230 ºC.

Conclusion

In this study, pure ZnO films were produced by the hydrothermal method based on dip-coated nucleation layers with 5 and 10 dipping cycles. XRD patterns revealed a well-defined crystal structure of hexagonal wurtzite ZnO at 5 dipping cycles. With the increase in the number of dipping cycles, the average crystallite size increased from 241 Å to 272 Å followed by a remarkable deformation in crystal structure manifested by the weak diffraction peaks spotted in the sample based on 10 dipping cycles. SEM images of the synthesized

samples showed an increase in the thickness of the coated seed layers from about 123 nm with 5 dipping cycles to 201 nm with 10 dipping cycles. With the hydrothermal treatment, the diameter of the rods to be formed increased from about 27 nm to 37 nm with the increase in the number of dipping cycles from 5 to 10. Such an increase in rod thickness caused a decrease in the surface area-to-volume ratio and porosity in the produced film. The fact that no well-formed rods were seen after the hydrothermal treatment was attributed to the insufficient reaction temperature (70 ºC) and reaction time (1 h) during the hydrothermal synthesis. The structural and morphological changes triggered by the number of dipping cycles in the seed layers influenced the gas sensing performance of the corresponding films. The optimal working temperature was not affected by the number of dipping cycles where both sensors showed a maximum response at about 230 ºC. However, the increment in the number of dipping cycles caused a decrease in the sensitivity of the sensor at all investigated operating temperatures and for all investigated gas concentrations, and was ascribed to the structural and morphological changes happened by the increase in the number of dipping cycles. This study emphasized once again the huge effect of synthesis parameters on the formation of nanostructured materials and particularly optimized the number of dipping cycles in seed layers for hydrothermal growth.

Acknowledgment

This study was financially supported by Gazi University Scientific Research Fund (project code: FOA-2021-7384).

Conflict of Interest

The authors declare that they have no conflict of interest.

References

Amudhavalli, B., Mariappan, R., & Prasath, M. (2022). Synthesis chemical methods for deposition of ZnO, CdO and CdZnO thin films to facilitate further research. *Journal of Alloys and Compounds*, *925*, 166511. https://doi.org/10.1016/j.jallcom.2022.166511

Altun, B., Karaduman Er, I., Çağırtekin, A. O., Ajjaq, A., Sarf, F., & Acar, S. (2021). Effect of Cd dopant on structural, optical and CO_2 gas sensing properties of ZnO thin film sensors fabricated by chemical bath deposition method. *Applied Physics A*, *127*, 687. https://doi.org/10.1007/s00339-021-04843-9

Al Farsi, B., Souier, T. M., Al Marzouqi, F., Al Maashani, M., Bououdina, M., Widatallah, H. M., & Al Abri, M. (2021). Structural and optical properties of visible active photocatalytic Al doped ZnO nanostructured thin films prepared by dip coating. *Optical Materials*, *113*, 110868. https://doi.org/10.1016/j.optmat.2021.110868

Atay, F., & Gultepe, O. (2021). The effect of spinning cycle on structural, optical, surface and photocatalytic properties of sol–gel derived ZnO films. *Journal of Sol-Gel Science and Technology*, *100*, 299-309. https://doi.org/10.1007/s10971-021-05661-4

Amin, G., Asif, M. H., Zainelabdin, A., Zaman, S., Nur, O., & Willander, M. (2011). Influence of pH, precursor concentration, growth time, and temperature on the morphology of ZnO nanostructures grown by the hydrothermal method. *Journal of Nanomaterials*, *2011*, 269692. https://doi.org/10.1155/2011/269692

Barin, Ö., Ajjaq, A., Çağırtekin, A. O., Karaduman Er, I., Yıldırım, M. A., Ateş, A., & Acar, S. (2022). Pivotal role of nucleation layers in the hydrothermally-assisted growth of ZnO and its H_2 gas sensing performance. *Sensors and Actuators B: Chemical*, *371*, 132499. https://doi.org/10.1016/j.snb.2022.132499

Cura, Ö., Ajjaq, A., Çağırtekin, A. O., Cavdar, S., & Acar, S. (2021). Low-energy ball milling effect on the dielectric response and electrical transport mechanisms of natural clinoptilolite zeolites in a wide temperature range. *Materials Today Communications*, *29*, 102964. https://doi.org/10.1016/j.mtcomm.2021.102964

Devi, K. R., Selvan, G., Karunakaran, M., Kanna, G. R., & Kasirajan, K. (2019). Role of dipping cycle on Mn doped ZnO thin films prepared by successive ionic layer adsorption and reaction method. *Sensor Letters*, *17*(12), 987-990. https://doi.org/10.1166/sl.2019.4171

Ghosh, A., Zhang, A. C., Ju, S., & Zhang, H. (2020). Selective H_2 sensing using lanthanum doped zinc oxide thin film: A study of temperature dependence H_2 sensing effect on carrier reversal activity. *AIP Journal of Applied Physics*, *128*(9), 094504. https://doi.org/10.1063/5.0012788

Gao, W., & Li, Z. (2004). ZnO thin films produced by magnetron sputtering. *Ceramics International*, *30*(7), 1155-1159. https://doi.org/10.1016/j.ceramint.2003.12.197

Kaya, S., Ozturk, O., & Arda, L. (2020). Roughness and bearing analysis of ZnO nanorods. *Ceramics International*, *46*(10A), 15183-15196. https://doi.org/10.1016/j.ceramint.2020.03.055

Kamruzzaman, M., & Zapien, J. A. (2018). Effect of temperature, time, concentration, annealing, and substrates on ZnO nanorod arrays growth by hydrothermal process on hot plate. *Crystallography Reports*, *63*, 456-471. https://doi.org/10.1134/S1063774518030112

Mohammad, S. M., Hassan, Z., Talib, R. A., Ahmed, N. M., Al-Azawi, M. A., Abd-Alghafour, N. M., Chin, C. W., & Al-Hardan, N. H. (2016). Fabrication of a highly flexible low-cost H_2 gas sensor using ZnO nanorods grown on an ultra-thin nylon substrate. *Journal of Materials Science: Materials in Electronics*, *27*, 9461-9469. https://doi.org/10.1007/s10854-016-4993-4

Poornajar, M., Marashi, P., Fatmehsari, D. H., & Esfahani, M. K. (2016). Synthesis of ZnO nanorods via chemical bath

deposition method: The effects of physicochemical factors. *Ceramics International*, *42*(1A), 173-184. https://doi.org/10.1016/j.ceramint.2015.08.073

Raghu, P., Srinatha, N., Mahesh, H. M., & Angadi, B. (2018). Transparent, crystalline ZnO thin films: Effect of spin coating parameters on the structural and optical properties. *AIP Conference Proceedings*, *1953*(1), 100052. https://doi.org/10.1063/1.5032988

Sansenya, T., Masri, N., Chankhanittha, T., Senasu, T., Piriyanon, J., Mukdasai, S., & Nanan, S. (2022). Hydrothermal synthesis of ZnO photocatalyst for detoxification of anionic azo dyes and antibiotic. *Journal of Physics and Chemistry of Solids*, *160*, 110353. https://doi.org/10.1016/j.jpcs.2021.110353

Soltabayev, B., Yergaliuly, G., Ajjaq, A., Beldeubayev, A., Acar, S., Bakenov, Z., & Mentbayeva, A. (2022). Quick NO gas sensing by Ti-doped flower–rod-like ZnO structures synthesized by the SILAR method. *ACS Applied Materials and Interfaces*, *14*(36), 41555-41570. https://doi.org/10.1021/acsami.2c10055

Saha, J. K., Bukke, R. N., Mude, N. N., & Jang J. (2020). Significant improvement of spray pyrolyzed ZnO thin film by precursor optimization for high mobility thin film transistors. *Scientific Reports*, *10*, 8999. https://doi.org/10.1038/s41598-020-65938-6

Toe, M. Z., Pung, S. Y., Binti Yaacob, K. A., & Han, S. S. (2021). Effect of dip-coating cycles on the structural and performance of ZnO thin film-based DSSC. *Arabian Journal for Science and Engineering*, *46*, 6741-6751. https://doi.org/10.1007/s13369-021-05418-9

Xu, J., Pan, Q., Shun, Y., & Tian, Z. (2000). Grain size control and gas sensing properties of ZnO gas sensor. *Sensors and Actuators B: Chemical*, *66*(1-3), 277-279. https://doi.org/10.1016/S0925-4005(00)00381-6